NASA TECHNICAL REPORT

NASA TR R-210

NASA TR R-210

ANGLE-OF-ATTACK CONVERGENCE OF SPINNING BODIES ENTERING PLANETARY ATMOSPHERES AT LARGE INCLINATIONS TO THE FLIGHT PATH

by Murray Tobak and Victor L. Peterson

Ames Research Center
Moffett Field, Calif.

NATIONAL AERONAUTICS AND SPACE ADMINISTRATION • WASHINGTON, D. C. • OCTOBER 1964

ANGLE-OF-ATTACK CONVERGENCE OF SPINNING BODIES ENTERING PLANETARY ATMOSPHERES AT LARGE INCLINATIONS TO THE FLIGHT PATH

By Murray Tobak and Victor L. Peterson

Ames Research Center
Moffett Field, Calif.

NATIONAL AERONAUTICS AND SPACE ADMINISTRATION

For sale by the Office of Technical Services, Department of Commerce,
Washington, D.C. 20230 -- Price $0.50

ANGLE-OF-ATTACK CONVERGENCE OF SPINNING BODIES ENTERING PLANETARY ATMOSPHERES AT LARGE INCLINATIONS TO THE FLIGHT PATH

By Murray Tobak and Victor L. Peterson

Ames Research Center
Moffett Field, Calif.

SUMMARY

An analysis is made of the angle-of-attack history of a spinning body entering a planetary atmosphere at an arbitrarily large inclination to the flight path. An asymptotic solution for the resultant angle of attack is derived, applicable to any axially symmetric body having an aerodynamic restoring-moment coefficient proportional to the sine of the resultant angle of attack. The solution yields results in satisfactory agreement with results obtained from numerical integrations of the exact equations of motion.

INTRODUCTION

In a recent analysis of the atmospheric-entry dynamics of spheroidal tektites (ref. 1), the authors were led to study the motions of a spinning body entering the atmosphere at an arbitrarily large inclination to the flight path. An expression for the history of the angle-of-attack envelope is offered without proof in reference 1 as a generalization of a useful result given previously by Leon in reference 2. The generalization retains the concise form of the original while removing the restriction to small initial inclinations; it is applicable to the motion of any axially symmetric body having an aerodynamic restoring-moment coefficient proportional to the sine of the resultant angle of attack.

Vehicles destined for use as planetary probes no doubt often will be spin-stabilized and, moreover, often will have profiles derivable from that of the spheroid. For such profiles, the aerodynamic restoring-moment coefficient will be reasonably well approximated by a function proportional to the sine of the angle of attack. Hence, the expression derived initially to explain the motions of tektites may apply directly to the motions of probe vehicles as well. In view of this, it is deemed advisable to present here a complete derivation and evaluation of the result cited in reference 1.

In connection with the nonlinear problem considered here, two antecedent papers, unknown to the authors during the preparation of this report, should also be cited.[1] Reference 3 contains a derivation of the nonlinear

---

[1]The authors are indebted to Mr. Percy J. Bobbitt for bringing these papers to their attention.

differential equation governing the angle-of-attack motion; the ensuing analysis, however, is devoted to the frequency and precession rate of the motion rather than the angle-of-attack envelope studied here. Reference 4 is addressed to the same problem as that of the present report, but the analysis does not lead to a solution having the concise functional form of the one presented here.

SYMBOLS

A	reference area
C_m	restoring-moment coefficient, $\frac{\text{restoring moment}}{QAl}$
f	dependent variable, $\tan \frac{\sigma}{2}$
G	parameter defined by equation (46)
h	altitude
I	moment of inertia about x' or y' axis
$I_{z'}$	moment of inertia about z' axis
i	$\sqrt{-1}$
$J_{-i\bar{\nu}}(x), J_{i\bar{\nu}}(x)$	Bessel functions of imaginary order
l	reference length
M	magnitude of aerodynamic moment vector
p,q,r	angular velocities about z', x', y' axes, respectively
Q	dynamic pressure, $\frac{1}{2}\rho V^2$
s	dynamic pressure parameter, $\beta V_i \sin \gamma_i$
t	time
V	flight velocity
X,Y,Z	axes having fixed directions in space, origin at center of gravity of body (sketch (a))
x	independent variable (eq. (20))
x',y',z'	axes fixed in body, origin at center of gravity (sketch (a))
y	dependent variable (eq. (31))
α	angle of attack in planar motion
β	density parameter (eq. (13))
γ	flight-path angle

κ value of x at $t = 0$, $\sqrt{\frac{-4}{s^2} Q_i \frac{Al}{I} C_{m_{max}}}$ (eq. (20))

λ $\frac{I_{z'} - I}{I}$

ν spin parameter, $\frac{p_i}{s} \frac{I_{z'}}{I}$

$\bar{\nu}$ modified spin parameter, $\nu \cos^2 \frac{\sigma_i}{2}$

ξ dependent variable, $\frac{f}{f_i}$

ρ density of planetary atmosphere

ρ_o density of planetary atmosphere at surface of planet

φ, ψ, σ Eulerian angles, with σ measuring resultant angle of attack (sketch (a))

ω complex angular velocity, $q + ir$

$(\dot{})$ $\frac{d}{dt}( )$

$( )'$ $\frac{d}{dx}( )$

$( )_i$ initial value

$(\bar{})$ complex conjugate of quantity

$( )_{max}$ maximum value of quantity

$( )_{min}$ minimum value of quantity

$( )_{env}$ envelope of oscillatory function

ANALYSIS

The following assumptions and approximations, common to references 1 and 2, are retained in the ensuing analysis:

(a) Rotation of planet and atmosphere are neglected.

(b) Aerodynamic damping terms are neglected, so that the aerodynamic moment coefficient is proportional to resultant angle of attack only.

(c) Flight-path angle γ and velocity V remain constant at their initial values γ_i and V_i.

Assumption (c) limits applicability of the analysis to the initial portion of the entry during which the dynamic pressure increases rapidly with time. It will be seen, however, that the end results can be cast in a form which circumvents this limitation.

As assumption (c) serves to define the motion of the center of gravity, only the motion of the body about the center of gravity need be considered. To this end, two orthogonal coordinate systems are affixed to the center of gravity as shown on sketch (a). The X, Y, Z axes are reference axes having fixed directions in space, the Z axis being alined with the direction of the velocity vector. The x', y', z' axes are principal axes fixed in the body, the z' axis being coincident with the body's longitudinal axis. The body has cylindrical symmetry about the z' axis so that, with products of inertia absent, $I_{x'} = I_{y'} = I$. The body axes are oriented relative to the reference axes by the Eulerian angles φ, ψ, σ, with σ measuring the resultant angle of attack. By assumption (b) and symmetry the aerodynamic force on the body lies in the σ plane. Hence, the aerodynamic moment about the center of gravity is a vector directed normal to the σ plane, or along the line of nodes. Let p, q, r be the components of angular velocity about the z', x', y' axes, respectively. The equations of motion are (ref. 5)

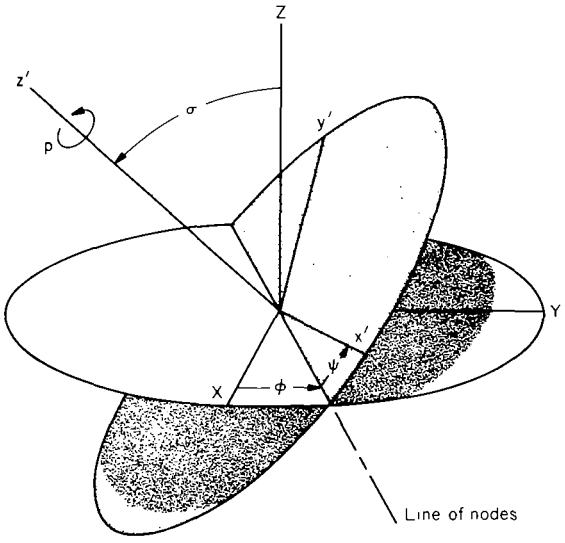

Z Flight path direction
z' Body axis of rotation
σ Resultant angle of attack

Sketch (a)

$$\left.\begin{aligned} I_{z'}\,\dot{p} &= 0 \\ I\dot{q} - (I - I_{z'})pr &= M(\sigma)\cos\psi \\ I\dot{r} + (I - I_{z'})pq &= -M(\sigma)\sin\psi \end{aligned}\right\} \quad (1)$$

where $M(\sigma)$ is the magnitude of the aerodynamic moment vector and where the relations between p, q, r and the Eulerian angles are (ref. 5)

$$\left.\begin{aligned} p &= \dot{\varphi}\cos\sigma + \dot{\psi} \\ q &= \dot{\varphi}\sin\sigma\sin\psi + \dot{\sigma}\cos\psi \\ r &= \dot{\varphi}\sin\sigma\cos\psi - \dot{\sigma}\sin\psi \end{aligned}\right\} \quad (2)$$

The first of equations (1) integrates immediately, showing that the roll rate p remains constant at p_i. The two remaining equations are combined by the formation of a complex angular rate ω,

$$\omega = q + ir \tag{3}$$

to give

$$\dot{\omega} - i\lambda p_i \omega = \frac{M(\sigma)}{I} e^{-i\psi} \tag{4}$$

where

$$\lambda = \frac{I_{z'} - I}{I} \tag{5}$$

Another expression for ω is obtained from equations (2), namely

$$\omega = e^{-i\psi}(\dot{\sigma} + i\dot{\phi} \sin \sigma) \tag{6}$$

Equation (6) and its derivative may be substituted in equation (4) to eliminate ω. There results a complex equation which may be broken into the two real equations

$$\ddot{\sigma} + \dot{\phi}(\lambda p_i + \dot{\psi}) \sin \sigma = \frac{M(\sigma)}{I} \tag{7a}$$

$$\frac{d}{dt}(\dot{\phi} \sin \sigma) - \dot{\sigma}(\lambda p_i + \dot{\psi}) = 0 \tag{7b}$$

Consider equation (7b). From equations (2)

$$\lambda p_i + \dot{\psi} = p_i(\lambda + 1) - \dot{\phi} \cos \sigma \tag{8}$$

Substituting equation (8) in (7b) and multiplying through by $\sin \sigma$ gives

$$\frac{d}{dt}(\dot{\phi} \sin^2 \sigma) = -p_i(\lambda + 1) \frac{d}{dt} \cos \sigma \tag{9}$$

which may be integrated to yield

$$\dot{\phi} = p_i(\lambda + 1)\left(\frac{\cos \sigma_i - \cos \sigma}{\sin^2 \sigma}\right) \tag{10}$$

where the initial condition $\dot{\phi}_i = 0$ has been invoked. The latter condition is consistent with the specification that initially the body axis z' have a fixed direction with respect to space-fixed coordinates. On the substitution of equations (8) and (10) in (7a) and some manipulation, a differential equation for σ alone is obtained of the following form

$$\ddot{\sigma} \sin^3 \sigma + 4p_i^2(\lambda + 1)^2 \left[\left(1 - 2 \sin^2 \frac{\sigma_i}{2}\right) \sin^4 \frac{\sigma}{2} - \left(1 - 2 \sin^2 \frac{\sigma}{2}\right) \sin^4 \frac{\sigma_i}{2}\right]$$

$$= \frac{M(\sigma)}{I} \sin^3 \sigma \qquad (11)$$

At this point, the aerodynamic pitching-moment coefficient $C_m(\sigma)$ is specified to be proportional to the sine of the resultant angle of attack; that is,

$$C_m(\sigma) = C_{m_{max}} \sin \sigma \qquad (12)$$

Further, as in references 1 and 2, the assumption that the density of the planetary atmosphere varies exponentially with altitude is introduced

$$\rho = \rho_o e^{-\beta h} \qquad (13)$$

which, together with assumption (c), gives for the dynamic pressure

$$Q = Q_i e^{st} \qquad (14)$$

where

$$\left.\begin{aligned} Q_i &= \frac{1}{2} \rho_o V_i^2 e^{-\beta h_i} \\ s &= \beta V_i \sin \gamma_i \end{aligned}\right\} \qquad (15)$$

Let

$$\left(\frac{\kappa s}{2}\right)^2 = -Q_i \frac{Al}{I} C_{m_{max}} \qquad (16)$$

so that

$$\frac{M(\sigma)}{I} = \frac{QAl}{I} C_m(\sigma) = -\left(\frac{\kappa s}{2}\right)^2 e^{st} \sin \sigma \qquad (17)$$

Also, let

$$\nu = \frac{p_i}{s} (\lambda + 1) = \frac{p_i}{s} \frac{I_z'}{I} \qquad (18)$$

Equation (11) becomes

$$\ddot{\sigma} \sin^3 \sigma + 4(\nu s)^2 \left[\left(1 - 2 \sin^2 \frac{\sigma_i}{2}\right) \sin^4 \frac{\sigma}{2} - \left(1 - 2 \sin^2 \frac{\sigma}{2}\right) \sin^4 \frac{\sigma_i}{2}\right]$$

$$+ \left(\frac{\kappa s}{2}\right)^2 e^{st} \sin^4 \sigma = 0 \qquad (19)$$

Finally, in conformity with reference 1, the new independent variable x is introduced

$$x = \kappa e^{st/2} \tag{20}$$

together with the transformation

$$f = \tan \sigma/2 \tag{21}$$

which bring equation (19) to

$$f''(x) - \frac{2ff'^2}{1 + f^2} + \frac{f'}{x} + f + \frac{\nu^2}{x^2}\left(\frac{1 + f^2}{1 + f_i^2}\right)^2\left(\frac{f^4 - f_i^4}{f^3}\right) = 0 \tag{22}$$

Fixing the initial inclination of the body z' axis with respect to space-fixed coordinates requires that the initial conditions on f be

$$\left.\begin{aligned} f_i &= f(\kappa) = \tan \sigma_i/2 \\ f_i' &= f'(\kappa) = 0 \end{aligned}\right\} \tag{23}$$

Equation (22) (with (23)) is the fundamental equation of this report.

Asymptotic Solution

An asymptotic solution of equation (22) will be obtained in a manner similar to that of reference 1. First, let us normalize the dependent variable by

$$\frac{f}{f_i} = \xi \tag{24}$$

and rearrange the differential equation so that

$$\xi'' + \frac{\xi'}{x} + \xi - \left(\frac{\nu}{1 + f_i^2}\right)^2 \frac{1 - \xi^4}{x^2\xi^3} = f_i^2\left[\frac{2\xi\xi'^2}{1 + f_i^2\xi^2} + \frac{\nu^2}{x^2}\frac{1 - \xi^4}{\xi}\frac{2 + f_i^2\xi^2}{(1 + f_i^2)^2}\right] \tag{25}$$

Equation (25) reveals that for small f_i (i.e., small σ_i), the right side becomes negligibly small and may be put to zero. The resulting equation can be solved exactly. This is the problem treated in reference 2. For larger values of f_i, an exact solution cannot be obtained. It can be shown, however, that for large x, the leading terms on the right side will die out as $x^{-3/2}$ whereas those on the left side will die out as $x^{-1/2}$. Hence, the left side of equation (25) will govern the asymptotic behavior of the solution. Note that, with f_i different from zero, the spin parameter ν on the left side is now modified by a factor dependent on initial inclination. Let the modified spin parameter be denoted by $\bar{\nu}$ where

$$\bar{\nu} = \frac{\nu}{1 + f_i^2} = \nu \cos^2 \sigma_i/2 \tag{26}$$

and, for brevity, let

$$g(x) = f_i^2 \left[\frac{2\xi\xi'^2}{1 + f_i^2\xi^2} + \frac{\nu^2}{x^2} \frac{1 - \xi^4}{\xi} \frac{2 + f_i^2\xi^2}{(1 + f_i^2)^2} \right] \tag{27}$$

so that equation (25) becomes

$$\xi'' + \frac{\xi'}{x} + \xi - \bar{\nu}^2 \frac{1 - \xi^4}{x^2\xi^3} = g(x) \tag{28}$$

Complex equation.- Equation (28) is now cast in a simpler form. It can be shown that the following pair of coupled equations is equivalent to equation (28):

$$\left.\begin{aligned} \epsilon'' + \frac{\epsilon'}{x} + \epsilon + 2\frac{\bar{\nu}}{x}\eta' &= g(x) \sin \mu \\ \eta'' + \frac{\eta'}{x} + \eta - 2\frac{\bar{\nu}}{x}\epsilon' &= g(x) \cos \mu \end{aligned}\right\} \tag{29}$$

where

$$\left.\begin{aligned} \epsilon &= \xi \sin \mu \\ \eta &= \xi \cos \mu \end{aligned}\right\} \tag{30}$$

Forming the complex function

$$y = \epsilon + i\eta \tag{31}$$

and adding in equations (29) gives a single equation

$$y'' + \frac{y'}{x}(1 - 2i\bar{\nu}) + y = g_1(x) \tag{32}$$

with

$$g_1(x) = ig(x)e^{-i\mu} \tag{33}$$

Having a solution for y, one obtains the desired solution for ξ^2 simply by forming the conjugate solution $\bar{y}$ and multiplying, for by equations (30) and (31)

$$\xi^2 = y\bar{y} \tag{34}$$

Asymptotic behavior.- The form of the left side of equation (32) suggests that the behavior of y will be similar to that of the Bessel function of imaginary order $J_{-i\bar{\nu}}(x)$. To put this in evidence, the method of

variation of parameters is used to cast equation (32) in the form of an integral equation involving the Bessel function. Thus, when the initial conditions of equations (23) are invoked,

$$y = x^r \left\{ aJ_{-r}(x) - \frac{\pi}{2} \int_\kappa^x \frac{u^{1-r}}{\sin \pi r} g_1(u) \Big[J_r(u)J_{-r}(x) - J_r(x)J_{-r}(u) \Big] du \right\} \tag{35}$$

with

$$a = ie^{-i\mu} i_2^{-r} \Gamma(1 - r)$$

$$r = i\bar{\nu}$$

For small f_i the integral may be discarded and the solution will be simply the first term. For arbitrary f_i, the asymptotic behavior of equation (35) is obtained as follows: Write equation (35) as

$$y = x^r \left\{ aJ_{-r}(x) - \frac{\pi}{2} \int_\kappa^\infty \frac{u^{1-r}}{\sin \pi r} g_1(u) \Big[J_r(u)J_{-r}(x) - J_r(x)J_{-r}(u) \Big] du \right.$$

$$\left. + \frac{\pi}{2} \int_x^\infty \frac{u^{1-r}}{\sin \pi r} g_1(u) \Big[J_r(u)J_{-r}(x) - J_r(x)J_{-r}(u) \Big] du \right\} \tag{36}$$

The second integral vanishes faster than $x^{-1/2}$ for $x \to \infty$ and hence may be discarded. Then the asymptotic behavior of $y(x)$ is

$$y \approx x^r \Big[a_1 J_{-r}(x) + b_1 J_r(x) \Big] \tag{37}$$

where

$$a_1 = a - \frac{\pi}{2} \int_\kappa^\infty \frac{u^{1-r}}{\sin \pi r} g_1(u) J_r(u) du$$

$$b_1 = \frac{\pi}{2} \int_\kappa^\infty \frac{u^{1-r}}{\sin \pi r} g_1(u) J_{-r}(u) du$$

The asymptotic behavior of the conjugate solution is

$$\bar{y} \approx x^{-r} \Big[\bar{a}_1 J_r(x) + \bar{b}_1 J_{-r}(x) \Big] \tag{38}$$

so that ξ^2 varies asymptotically as

$$\xi^2 \approx (a_1\bar{a}_1 + b_1\bar{b}_1)J_r(x)J_{-r}(x) + a_1\bar{b}_1J_{-r}^2(x) + \bar{a}_1b_1J_r^2(x) \tag{39}$$

A more convenient form for ξ^2 is obtained when the expression is normalized with respect to the solution for small f_i. Thus

$$\xi^2 \approx \left[\frac{a_1\bar{a}_1 + b_1\bar{b}_1}{a\bar{a}} + \frac{a_1\bar{b}_1J_{-r}^2(x) + \bar{a}_1b_1J_r^2(x)}{a\bar{a}J_r(x)J_{-r}(x)}\right]a\bar{a}J_r(x)J_{-r}(x) \tag{40}$$

Envelope curves.- In order to find the envelope curves, the Bessel functions in equation (40) are replaced by the leading terms of their asymptotic expansions. The possibility of $\bar{\nu}$ being large is covered if the asymptotic expansions appropriate to simultaneously large $\bar{\nu}$ and x are used. From reference 6, one obtains

$$\left.\begin{aligned} J_{-i\bar{\nu}}(x) &\approx \sqrt{\frac{2}{\pi\sqrt{x^2 + \bar{\nu}^2}}}\cos\left(\varphi + \frac{\pi i}{2}\bar{\nu}\right) \\ J_{i\bar{\nu}}(x) &\approx \sqrt{\frac{2}{\pi\sqrt{x^2 + \bar{\nu}^2}}}\cos\left(\varphi - \frac{\pi i}{2}\bar{\nu}\right) \end{aligned}\right\} \tag{41}$$

with

$$\varphi = \sqrt{x^2 + \bar{\nu}^2} - \frac{\pi}{4} - \bar{\nu}\sinh^{-1}\frac{\bar{\nu}}{x} \tag{42}$$

Then

$$a\bar{a}J_{-i\bar{\nu}}(x)J_{i\bar{\nu}}(x) \approx \frac{2}{\pi\sqrt{x^2 + \bar{\nu}^2}}\Gamma(1 - i\bar{\nu})\Gamma(1 + i\bar{\nu})\left(\cosh^2\frac{\pi\bar{\nu}}{2} - \sin^2\varphi\right) \tag{43}$$

Since

$$\Gamma(1 - i\bar{\nu})\Gamma(1 + i\bar{\nu}) = \frac{\pi\bar{\nu}}{\sinh\pi\bar{\nu}} \tag{44}$$

equation (43) becomes

$$a\bar{a}J_{-i\bar{\nu}}(x)J_{i\bar{\nu}}(x) \approx \frac{2}{\pi\sqrt{x^2 + \bar{\nu}^2}}\left(\frac{\pi\bar{\nu}/2}{\tanh\pi\bar{\nu}/2}\right)\left[1 - \frac{\sin^2\varphi}{\cosh^2\pi\bar{\nu}/2}\right] \tag{45}$$

The quantity in brackets is a positive oscillatory function of constant amplitude, varying within the limits $\tanh^2\pi\bar{\nu}/2$ and unity. Now consider the quantity in brackets in equation (40). When the Bessel functions are replaced by equations (41), the convergence factor $(x^2 + \bar{\nu}^2)^{-1/2}$ is seen to occur in both the numerator and denominator of the second term. Hence, this factor cancels, so that the quantity in brackets also is a positive oscillatory function of constant amplitude. Let

$$G^2 = \left[\frac{a_1\bar{a}_1 + b_1\bar{b}_1}{a\bar{a}} + \frac{a_1\bar{b}_1 J_{-r}^2(x) + \bar{a}_1 b_1 J_r^2(x)}{a\bar{a} J_r(x) J_{-r}(x)}\right]\left(1 - \frac{\sin^2\varphi}{\cosh^2 \pi\bar{\nu}/2}\right) \qquad (46)$$

As each factor in equation (46) is a positive oscillatory function of constant amplitude, so is their product.[2] Equation (46) reveals that there will be two positive envelope curves for ξ, a maximum and a minimum. This is as it should be: The resultant angle of attack σ is always positive; when it is also oscillatory, it is clear that there must be a positive lower bound to the oscillation as well as an upper one. From equations (45) and (46), the envelope curves take the form

$$\left.\begin{aligned}(\xi)_{\max\ env} &= \sqrt{\frac{2}{\pi\sqrt{x^2 + \bar{\nu}^2}}}\sqrt{\frac{\pi\bar{\nu}/2}{\tanh \pi\bar{\nu}/2}}\, G_{\max}(\sigma_i, \nu) \\ (\xi)_{\min\ env} &= \sqrt{\frac{2}{\pi\sqrt{x^2 + \bar{\nu}^2}}}\sqrt{\frac{\pi\bar{\nu}/2}{\tanh \pi\bar{\nu}/2}}\, G_{\min}(\sigma_i, \nu)\end{aligned}\right\} \qquad (47)$$

It remains to determine the parameters G_{max} and G_{min}. This must be done numerically, and sketch (b) indicates the appropriate procedure. The exact variation of ξ with x is obtained from numerical integration of equation (25). When the product $(x^2 + \bar{\nu}^2)^{1/4}\xi$ is formed and plotted against x, the curve will approach a constant amplitude oscillation with increasing x. The upper and lower bounds of the oscillation, which are proportional to G_{max} and G_{min}, are easily measured from the figure. Curves of G_{max} and G_{min}/G_{max} as functions of σ_i are presented on figures 1 and 2 for a range of values of the spin parameter ν. To aid in interpolation, the parameters are also presented on figures 3 and 4 as functions of ν for several values of σ_i. Having G_{max}, G_{min}, and equation (47), one can determine the envelope curves of the physical variable σ. Invoking equations (21) and (24) casts equation (47) in the form

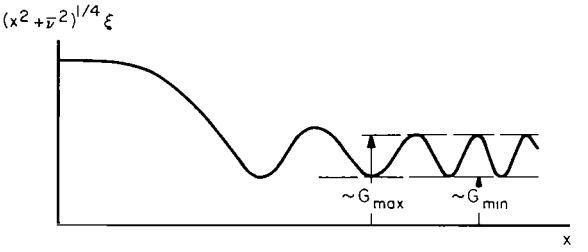

Sketch (b)

[2] An apparent contradiction with a result of reference 3 should be resolved here. It is indicated in reference 3 that the oscillation frequency for small σ_i may not be given correctly by the linear theory except in a certain special case. In contrast, equation (46) indicates that as $\sigma_i \to 0$ the linear theory does give the correct result, for as $\sigma_i \to 0$ the first factor in equation (46) approaches unity leaving the second factor, the linear theory result, to describe the frequency. The contradiction is resolved, however, when it is noted that the problem under study, wherein the body's axis of spin is initially fixed with respect to space-fixed coordinates (i.e., no wobble) is just the special case noted in reference 3 for which the linear theory does in fact give the correct result for frequency as $\sigma_i \to 0$.

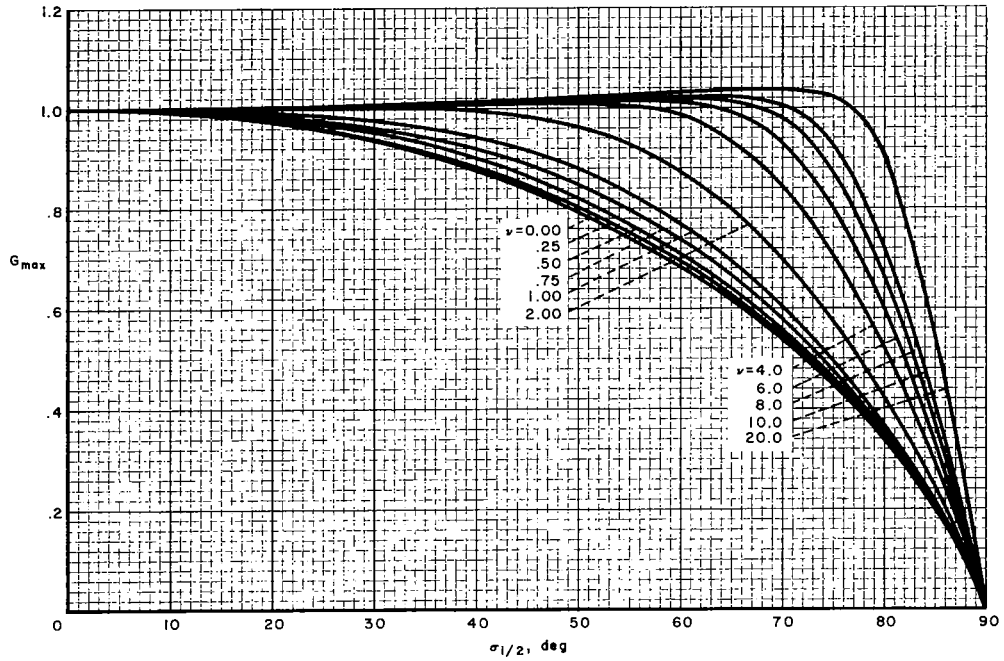

Figure 1.- Variation of the parameter G_{max} with initial inclination for several values of the spin parameter ν.

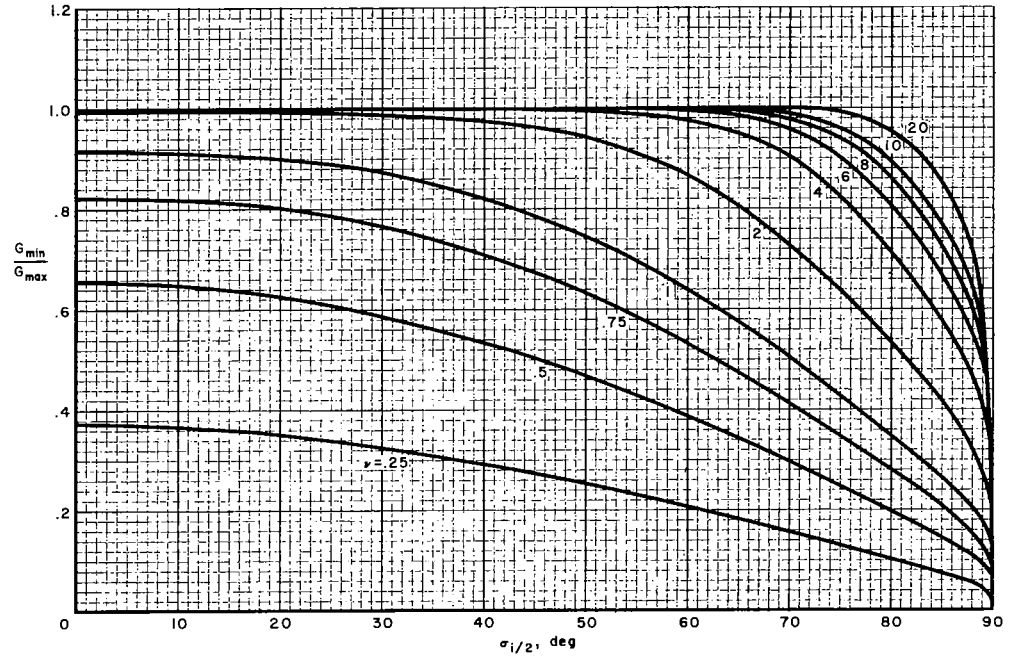

Figure 2.- Variation of the parameter G_{min}/G_{max} with initial inclination for several values of the spin parameter ν.

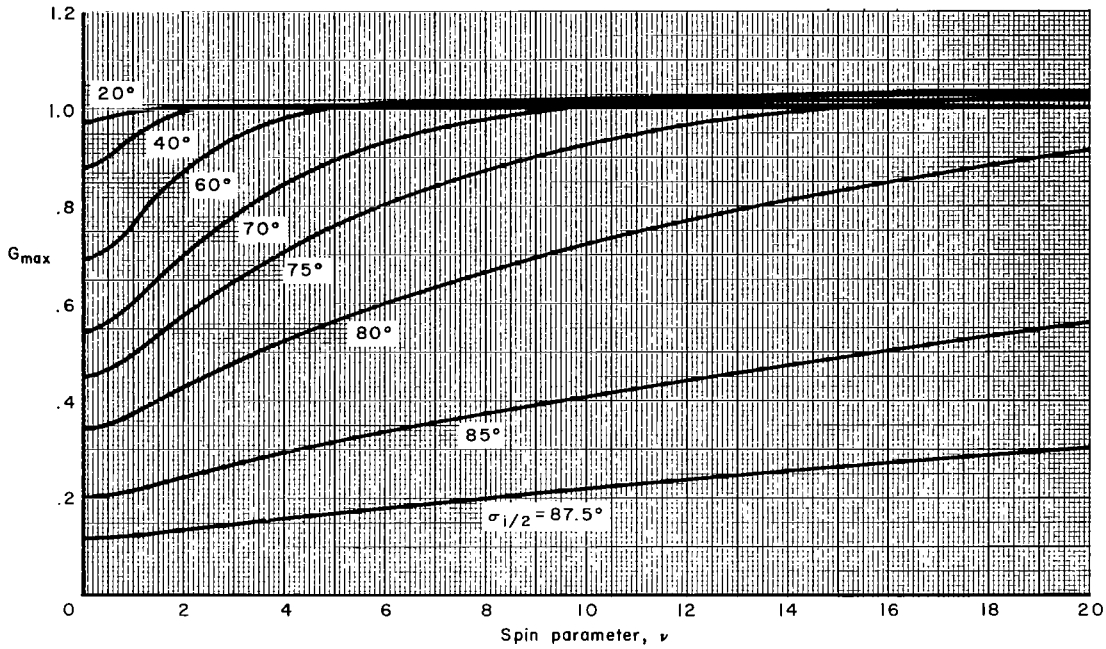

Figure 3.- Variation of the parameter G_{max} with the spin parameter ν for several values of the initial inclination σ_i.

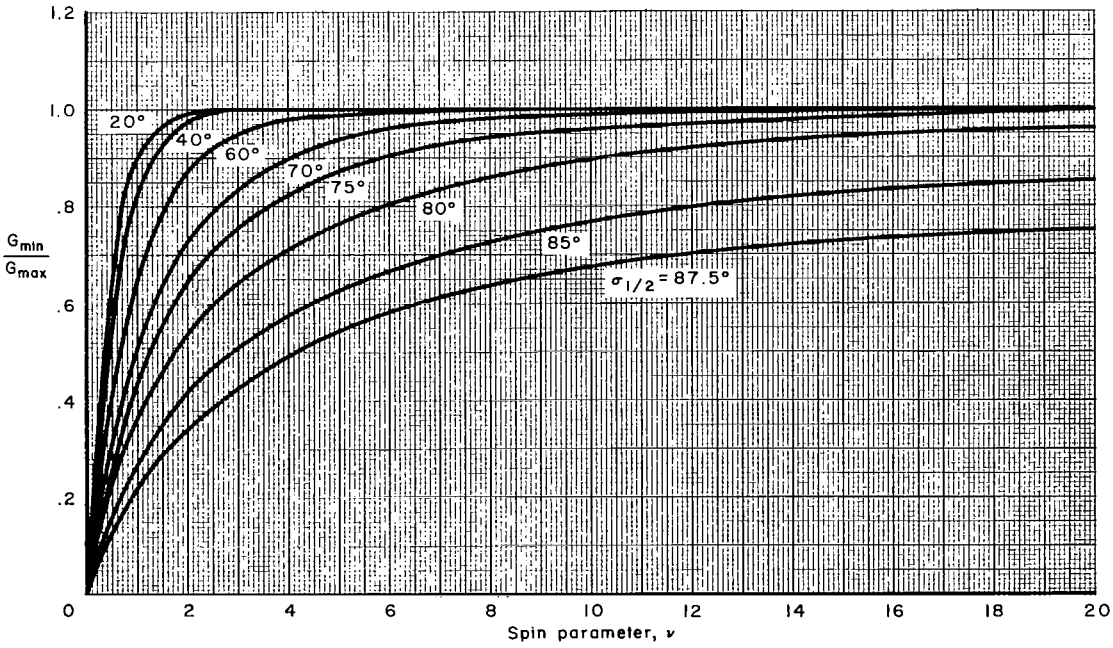

Figure 4.- Variation of the parameter G_{min}/G_{max} with the spin parameter ν for several values of the initial inclination σ_i.

$$\left.\begin{aligned}\frac{(\tan \sigma/2)_{\max\ env}}{\tan \sigma_i/2} &= \sqrt{\frac{2}{\pi\sqrt{x^2+\bar{\nu}^2}}}\sqrt{\frac{\pi\bar{\nu}/2}{\tanh\ \pi\bar{\nu}/2}}\, G_{max}(\sigma_i,\nu)\\ \frac{(\tan \sigma/2)_{\min\ env}}{\tan \sigma_i/2} &= \sqrt{\frac{2}{\pi\sqrt{x^2+\bar{\nu}^2}}}\sqrt{\frac{\pi\bar{\nu}/2}{\tanh\ \pi\bar{\nu}/2}}\, G_{min}(\sigma_i,\nu)\end{aligned}\right\} \tag{48}$$

Finally, the expedient adopted in reference 1 to extend the applicability of the results may be adopted here as well. The coordinate x is related to dynamic pressure through equations (14) and (20), namely

$$x = \kappa\sqrt{Q/Q_i} \tag{49}$$

When equation (49) is substituted in equations (48) the form agrees (for negligible aerodynamic damping and $\tanh \pi\nu/2 \approx 1$) with the asymptotic form given in reference 7 for the case of small σ_i. The result of reference 7, a more general one than that of reference 2, is independent of assumptions concerning flight-path angle or flight speed. Hence, in spite of the restrictions regarding these quantities underlying the development of equations (48) ($\gamma = \gamma_i$, $V = V_i$), the equations should yield an accurate representation of the asymptotic behavior even when V and γ are not constant if, after replacing x^2 in equations (48) by $\kappa^2 Q/Q_i$, one replaces Q/Q_i by a more precise expression than equation (14).

Envelope curves for small ν.- For small to moderate values of ν (i.e., $\bar{\nu}^2 \ll x^2$), equations (48) take the form

$$\frac{(\tan \sigma/2)_{\max\ env}}{\tan \sigma_i/2} = \sqrt{\frac{2}{\pi x}}\sqrt{\frac{\pi\bar{\nu}/2}{\tanh\ \pi\bar{\nu}/2}}\, G_{max}(\sigma_i,\nu) \tag{50a}$$

$$\frac{(\tan \sigma/2)_{\min\ env}}{\tan \sigma_i/2} = \sqrt{\frac{2}{\pi x}}\sqrt{\frac{\pi\bar{\nu}/2}{\tanh\ \pi\bar{\nu}/2}}\, G_{min}(\sigma_i,\nu) \tag{50b}$$

Consider the maximum envelope and now let ν be identically zero. The resulting motion is planar; let the angle of attack for planar motion be designated by the symbol α. Thus

$$\frac{(\tan \alpha/2)_{env}}{\tan \alpha_i/2} = \sqrt{\frac{2}{\pi x}}\, G_{max}(\sigma_i,0) \tag{51}$$

This is the envelope curve for a nonspinning body which enters the atmosphere at the initially fixed inclination α_i. The result checks equation (30) of reference 1. The ratio of equations (50a) and (51) for the same initial inclination ($\sigma_i = \alpha_i$) gives

$$\frac{(\tan \sigma/2)_{\max\ env}}{(\tan \alpha/2)_{env}} = \sqrt{\frac{\pi\bar{\nu}/2}{\tanh\ \pi\bar{\nu}/2}}\,\frac{G_{max}(\sigma_i,\nu)}{G_{max}(\sigma_i,0)} \tag{52}$$

As will be evident from figure 1, $G_{max}(\sigma_i, \nu)$ does not change significantly for small changes in ν. Hence, the ratio involving G_{max} in equation (52) is essentially unity. The result shows that for small ν, the envelope curve of the spinning body is increased over that of the nonspinning body by a constant factor dependent only on $\bar{\nu}$. This is the result reported in reference 1 which generalizes to large inclinations a prior result given in reference 2.

DISCUSSION

Results of the analysis will be discussed as they apply in particular to the motions of planetary probe vehicles. In addition, their accuracy will be indicated in the form of comparisons with results obtained by numerical integrations of the exact equations of motion.

Consider first the relationship between the maximum envelope of the resultant angle of attack for a spinning body and the envelope for a nonspinning body. Equation (52) shows this relationship to be independent of the coordinate x, and hence of the body's aerodynamic characteristics, so long as the square of the modified spin parameter is much less than the square of the coordinate ($\bar{\nu}^2 \ll x^2$). The results of reference 1 can be used to show that x generally becomes very large before the aerodynamic and heating loads reach large fractions of their maximum values. Over the latter portion of the trajectory, the portion of prime interest, the inequality will hold; hence it is appropriate to use equation (52) to illustrate the effects of spin. The results are presented on figure 5 for several values of the initial

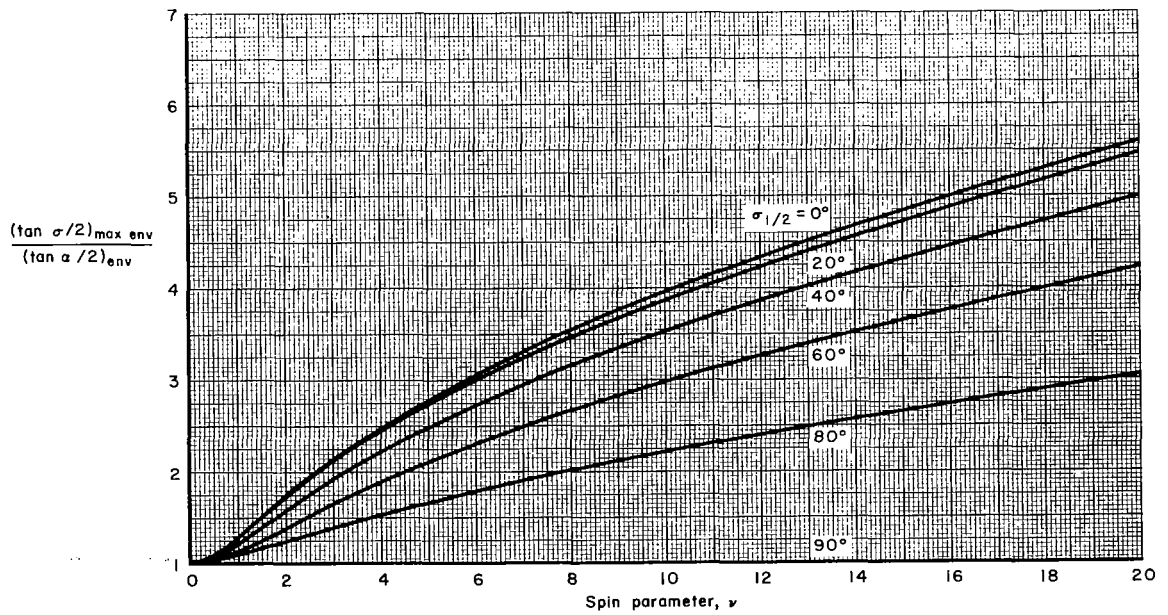

Figure 5.- Effect of spin on the maximum envelope of the resultant angle of attack.

inclination. They give a useful measure of the penalty factor attached to spin-stabilization, namely, a widening of the angle-of-attack envelope beyond that of the nonspinning body. The curve shown for small initial angles ($\sigma_i \to 0$) is identical to the result presented in reference 2; the penalty factor, which increases essentially as $\nu^{1/2}$, is seen to be a maximum for this case. For larger values of the initial angle, the penalty factor falls off from this curve essentially as $\cos \sigma_i/2$.

Now consider the relationship between the minimum and maximum envelopes for the spinning body. Forming the ratio $(\tan \sigma/2)_{\min \text{ env}}/(\tan \sigma/2)_{\max \text{ env}}$, one notes from equations (48) that it is just the ratio $G_{\min}(\sigma_i,\nu)/G_{\max}(\sigma_i,\nu)$, which already has been plotted as figures 2 and 4. The latter figure shows that the ratio rapidly approaches unity with increasing ν, essentially as $\tanh \pi\bar{\nu}/2$. The foregoing results suggest the following description of the motion: The angle σ in effect traces the movement of the body nose about the velocity vector. Initially, σ is fixed in value and the plane containing σ is fixed in inclination, but as the body penetrates deeper into the atmosphere σ begins to diminish while the σ plane begins to rotate about Z. Thus an observer on the Z axis sees the body nose trace out a diminishing spiral. The amplitude of successive turns of the spiral diminishes in accordance with the convergence factor $(x^2 + \bar{\nu}^2)^{-1/4}$. For small values of the spin parameter ν the motion is nearly planar, so that the spiral has a large eccentricity (i.e., $G_{\min}/G_{\max} \to 0$). Larger values of ν cause the spiral to open out so that each turn becomes nearly circular (i.e., $G_{\min}/G_{\max} \to 1$). Here, the merging of the envelopes means that the envelope curve itself becomes the actual angle-of-attack history. The effect of increasing σ_i, for a fixed value of ν, is to give the spiral a greater eccentricity; alternatively, larger values of spin rate are required to make the turns circular as the initial angle is increased.

Results of the analysis, shown in the form of variation of the resultant angle-of-attack envelopes with stagnation-point heating rate, are compared in figure 6 with results obtained by numerical methods. The latter results, in which no approximations were made either to the equations of motion or to the aerodynamic forces and moments, were obtained from the equations, entry conditions, and vehicle and planetary properties given in reference 8; the results are considered illustrative of those anticipated for a Mars entry. For the analytic results, the magnitude $C_{m_{max}}$ of the aerodynamic restoring-moment coefficient had to be specified in order to relate the coordinate x to aerodynamic heating rate in the manner indicated in reference 1. The value of $C_{m_{max}}$ was chosen such that the area under a half-cycle of the approximating sine function curve equalled that under the experimentally determined pitching-moment curve for the vehicle studied in reference 8. The values used for $C_{m_{max}}$ and those for other physical properties of the vehicle are given here for reference (cf., also sketch (c)):

$$C_{m_{max}} = -0.162$$

$$A = 8.296 \text{ ft}^2$$

$$I_{z'} = 2.8 \text{ lb-ft-sec}^2$$

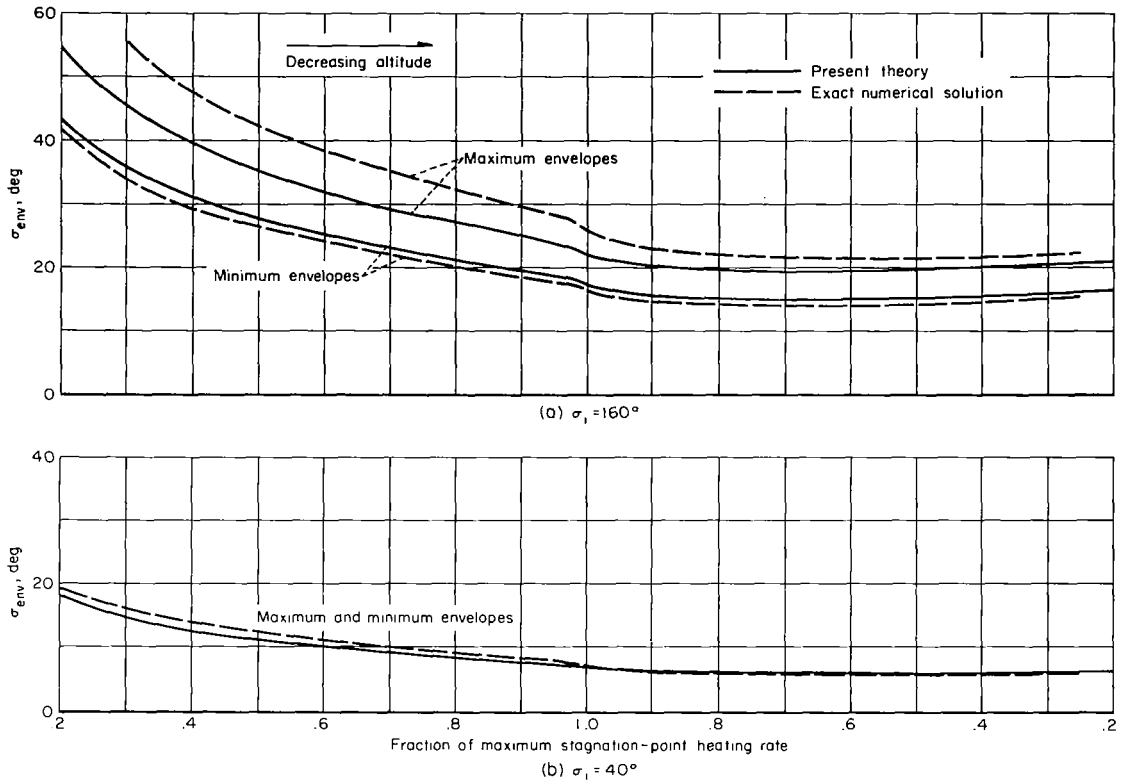

Figure 6.- Angle-of-attack envelopes as a function of fraction of maximum heating rate for a Mars entry; spin rate = 30 rpm.

$I = 5.6$ lb-ft-sec^2

$l = 3.25$ ft

$m = 6.685$ lb-sec^2/ft

$C_D = 0.650$

The martian atmosphere and other entry conditions are given as:

$\beta = 2.15 \times 10^{-5}$ per ft

$V_i = 21{,}042$ ft/sec

$\gamma_i = 41.5^\circ$

so that

$s = \beta V_i \sin \gamma_i = 0.30$ per sec

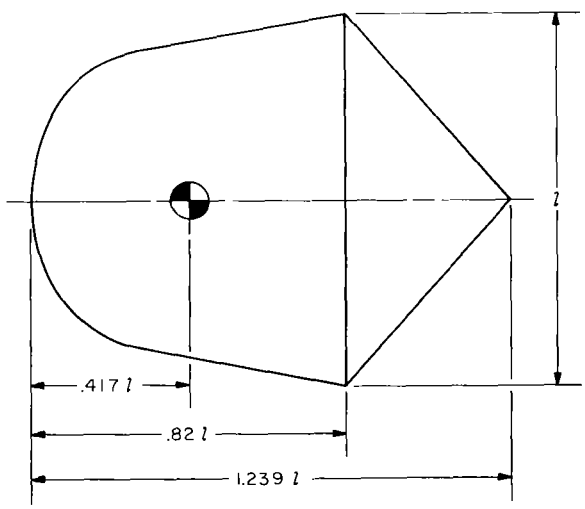

Sketch (c)

Agreement between numerically and analytically determined results for the angle-of-attack envelopes is seen to be satisfactory. Note that the maximum and minimum envelopes coincide for the conditions chosen for figure 6(b). In this case, the envelope curves shown represent actual angle-of-attack histories.

Additional comparisons are made in figure 7 which shows the effect of spin rate on the maximum envelope of resultant angle of attack at the point

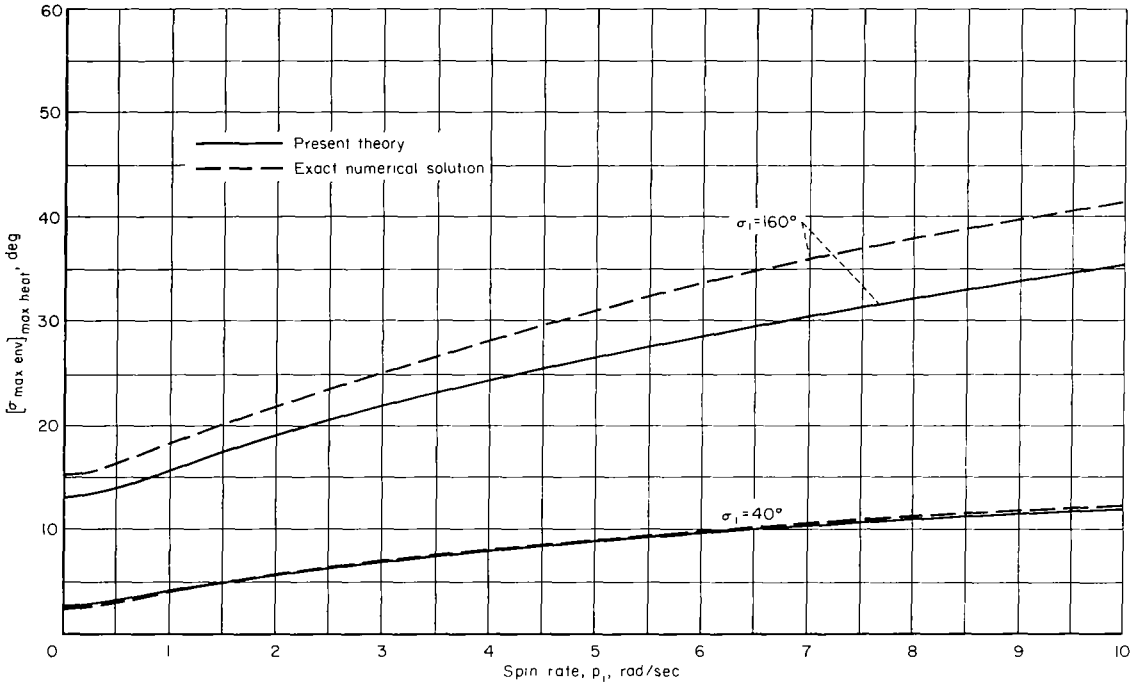

Figure 7.- Effect of spin on the maximum envelope of the resultant angle of attack; evaluated at point on a Mars entry trajectory where stagnation-point heating rate is maximum.

in the trajectory where stagnation-point heating rate is maximum. Satisfactory agreement between analytical and numerical results is indicated over the entire range chosen for the spin parameter.

CONCLUDING REMARKS

An analysis has been made of the angle-of-attack history of a spinning body which enters a planetary atmosphere at an arbitrarily large inclination to the flight path. An asymptotic solution for the resultant angle of attack was derived in a form that illustrates its functional dependence on vehicle and planetary properties. The solution applies to any axially symmetric body having an aerodynamic restoring-moment coefficient proportional to the sine of the resultant angle of attack. The solution was found to yield results in satisfactory agreement with results obtained from numerical integrations of the exact equations of motion.

Ames Research Center
National Aeronautics and Space Administration
Moffett Field, Calif., July 14, 1964

REFERENCES

1. Tobak, Murray, and Peterson, Victor L.: Theory of Tumbling Bodies Entering Planetary Atmospheres With Application to Probe Vehicles and the Australian Tektites. NASA TR R-203, 1964.

2. Leon, Herman I.: Angle of Attack Convergence of a Spinning Missile Descending Through the Atmosphere. Jour. Aero/Space Sci., vol. 25, no. 8, Aug. 1958, pp. 480-484.

3. Longmire, Conrad L.: Re-Entry of Rotating Missiles. Avco Corporation Research Note 213, Dec. 1960.

4. Albini, F. A.: Oscillation Envelope for a Spinning Re-Entry Vehicle. Hughes Corporation, Space Systems Division, Rep. No. 2183S, Feb. 27, 1962.

5. Goldstein, Herbert: Classical Mechanics. Addison-Wesley Publishing Company, Inc., Mass., 1959.

6. Watson, George N.: Theory of Bessel Functions. Second ed., Cambridge University Press, England, 1952.

7. Garber, T. B.: On the Rotational Motion of a Body Re-Entering the Atmosphere. Jour. Aero/Space Sci., vol. 26, no. 7, July 1959, pp. 443-449.

8. Peterson, Victor L.: Motions of a Short 10° Blunted Cone Entering a Martian Atmosphere at Arbitrary Angles of Attack and Arbitrary Pitching Rates. NASA TN D-1326, 1962.